Received: 15 January 2021 | Revised: 11 February 2021 | Accepted: 15 February 2021

DOI: 10.1002/nano.202100019

REVIEW

Nano Select Open Access WILEY

Coal based carbon dots: Recent advances in synthesis, properties, and applications

Ziguo He[1,2] | Shengjun Liu[1] | Cheng Zhang[1] | Liyuan Fan[3] | Jian Zhang[1] | Qian Chen[1] | Yudie Sun[1] | Lifang He[1] | Zhicai Wang[1] | Kui Zhang[1]

[1] School of Chemistry and Chemical Engineering, Anhui University of Technology, Ma'anshan, Anhui 243032, China

[2] Engineering Technology Research Center of Optoelectronic Technology Appliance, School of Mechanical Engineering, Tongling University, Tongling, Anhui 244061, China

[3] College of Science & Engineering, James Cook University, 1 James Cook Drive, Townsville, Queensland 4811, Australia

Correspondence
Cheng Zhang, Zhicai Wang, and Kui Zhang, School of Chemistry and Chemical Engineering, Anhui University of Technology, Ma'anshan, Anhui, 243032, China
Email: czhang@ahut.edu.cn (C. Z.), zhicaiw@ahut.edu.cn (Z. C. W.), zhangkui@mail.ustc.edu.cn (K. Z.)

Funding information
National Natural Science Foundation of China, Grant/Award Numbers: 21976002, 22004003, 21675158, 61603001; Anhui Provincial Natural Science Foundation for Distinguished Young Scholars, Grant/Award Number: 2008085J11

Abstract

Carbon dots are zero-dimensional carbon nanomaterials with quantum confinement effects and edge effects, which have aroused great interests in many disciplines such as energy, chemistry, materials, and environmental applications. They can be prepared by chemical oxidation, electrochemical synthesis, hydrothermal preparation, arc discharge, microwave synthesis, template method, and many other methods. However, the raw materials' high cost, the complexity and environmental-unfriendly fabrication process limit their large-scale production and commercialization. Herein, we review the latest developments of coal-based carbon dots about selecting coal-derived energy resources (bituminous coal, anthracite, lignite, coal tar, coke, etc.) the developments of synthesis processes, surface modification, and doping of carbon dots. The coal-based carbon dots exhibit the advantages of unique fluorescence, efficient catalysis, excellent water solubility, low toxicity, inexpensive, good biocompatibility, and other advantages, which hold the potentiality for a wide range of applications such as environmental pollutants sensing, catalyst preparation, chemical analysis, energy storage, and medical imaging technology. This review aims to provide a guidance of finding abundant and cost-effective precursors, green, simple and sustainable production processes to prepare coal-based carbon dots, and make further efforts to exploit the application of carbon dots in broader fields.

KEYWORDS
carbon dots, catalysis, coal, energy storage, fluorescence, sensing

1 | INTRODUCTION

Carbon is one of the most important elements in nature with various hybrid orbitals such as sp, sp^2, and sp^3,[1,2] which exists widely in the atmosphere, crust, and organisms in various forms. More and more carbon nanomaterials have been discovered, such as carbon nanotubes (CNTs),[3–5] graphite,[6] carbon fibers,[7,8] fullerenes,[9] and graphene.[10,11] Scientists have gradually found that carbon nanomaterials are superior to other materials in hardness, optical properties, heat resistance, radiation resistance, chemical resistance, electrical insulation,

conductivity, surface, and interface properties. Furthermore, Xu et al. firstly found Photoluminescence (PL) phenomenon in the process of purification of single-walled CNTs by arc discharge method in 2004.[12] Later, Sun et al. named the fluorescent carbon particles as Carbon Dots (CDs).[13] CDs are a new kind of zero-dimensional carbon nanomaterials, which represented by Carbon Quantum Dots (CQDs), Graphene Quantum Dots (GQDs), Carbonized Polymer Dots (CPDs),[14–20] and composed of carbon core and large oxygen-containing functional groups/polymer chains.[21,22] Due to the advantages of low toxicity, good biocompatibility, high chemical stability, and excellent photophysical properties,[23–33] CDs have been widely used in biological imaging,[31,34–38] ion detection,[32,39–43] photocatalysis,[27,44,45] and optoelectronic devices.[28–30,46–49]

The processes of CDs synthesis can be divided into two types, "top-down" and "bottom-up" methods.[50–59] Most traditional technologies used expensive carbon materials as the precursors to prepare CDs, such as CNTs, graphite, fullerene, carbon fiber, carbon black, graphene, and Graphene Oxide (GO).[60–64] Coal, as an important fossil fuel made up of large aromatic rings and thick aliphatic chains, has attracted researchers' attention, attributing to its affordability, abundant-earth, and high content carbon.[65] In 2013, Ye et al. fabricated the coal-based CDs with a controllable structure for the first time.[66] In recent years, scientists have made great breakthroughs in quantum-confinement,[67] edge effects,[67] defects (internal and external),[68] surface modification/passivation of coal-based CDs.[69–79]

This review introduces and summarizes the latest development of coal-based CDs in both theoretical and experimental aspects. In Part 2, the precursors (coal and its derivatives), synthesis methods, and physicochemical properties are discussed. Their applications in energy, environment, and biomedicine are discussed in Part 3. Furthermore, the challenges and prospects of the future development of coal-based CDs are discussed in Part 4.

2 | SYNTHESIS AND PROPERTIES OF COAL-BASED CDS

According to the degree of carbonization and processing technology, the precursors of coal-based CDs can be mainly divided into two categories: raw coals including bituminous coal, anthracite and lignite; and coal derivatives including coke and coal tar.

2.1 | Bituminous coal

Ye et al. reported the fabrication of GQDs from the bituminous coal (b-GQDs) by a facile one-step wet chemistry route (Figure 1A), generally including mixed acid (sulfuric acid [H_2SO_4] and nitric acid [HNO_3]) oxidation, stirring, oil bath heating (100°C), and neutralization (sodium hydroxide).[66] The size of the crystalline hexagonal GQDs was 2.96 ± 0.96 nm, the thickness was 1.5–3 nm, and the intensity ratio of defect signal (D) to graphitic order (G) peak (I_D/I_G) was 1.55 ± 0.19. With the rise of oxidation temperature to 120°C, the size of GQDs decreased to 2.30 ± 0.78 nm. The b-GQDs exhibited size- and pH-dependent PL in aqueous solutions (Figure 1B, C). The smaller the size of GQDs, the blue shift of emission wavelength. The stronger the acidity of GQDs solution, the blue shift of emission peak occurred. The stronger the alkalinity of GQDs solution, the redshift of emission peak took place. By applying high frequency (239.2 and 336 GHz) electron spin resonance spectroscopy, they found four distinct magnetic defect centers in the prepared b-GQDs.[68] Two of them were intrinsic carbon-core defects (broad signal: width = 697 [10^{-4} T], g = 2.0023; narrow signal: width = 60 [10^{-4} T], g = 2.003), and the other defect centers were Mn^{2+} (signal width = 61 [10^{-4} T], g = 2.0023, A_{iso} = 93 [10^{-4} T]) and copper ions (Cu^{2+}) ($g_{\perp}$ = 2.048 and $g_{\parallel}$ = 2.279), which influenced the properties of CDs.

Dong et al. reported the preparation of $Coal_A$ (mainly composed of single-layer GQDs with the average size and height of 10 and 0.5 nm) and $Coal_B$ (including agglomerated GQDs, GO, CQDs, and agglomerated carbon nanocrystals) by HNO_3 oxidation (Figure 2).[80] It was found that with the decrease of coalification degree, the yield of $Coal_A$ decreased from 56.30% to 14.66%. When the potential was cycled between −1.5 and +1.8 V (pH 7), the electroluminescence (ECL) performance of GQDs was significantly improved by adding $S_2O_8^{2-}$. Zhang and coworkers also reported the fabrication of GQDs containing a large number of hydroxyl (-OH), carboxyl (-COOH), aldehydes, carbonyls (-C = O) and ether bond (C-O-C) functional groups from bituminous coal by chemical oxidation of mixed acid (H_2SO_4 and HNO_3), and the size of b-GQDs ranged from 2 to 3.2 nm.[81] Recently, Hower et al. synthesized b-CQDs with a size distribution of 2–12 nm by an ultrasonic-assisted wet-chemical method in the presence of hydrogen peroxide (H_2O_2).[82] The quantum yield (QY) of b-CQDs was 0.53%, and the obtained b-CQDs emitted bright blue fluorescence at 365 nm excitation wavelength.

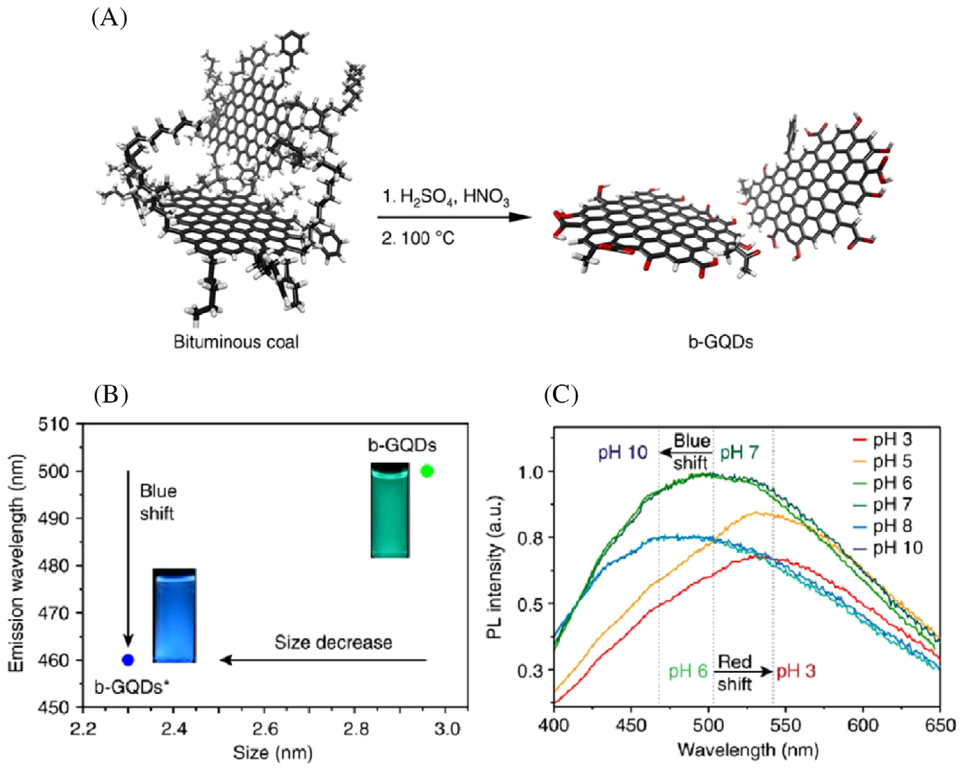

FIGURE 1 A, Schematic illustration of the synthesis of b-GQDs; the relationship between PL emission wavelength and the size of b-GQDs (B) and pH (C). Reproduced with permission.[66] Copyright, 2013, Springer Nature

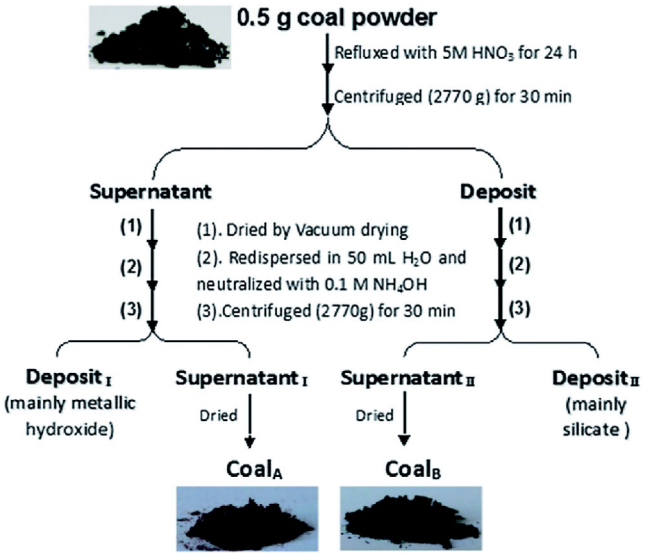

FIGURE 2 Treatment procedures of coal samples. Reproduced with permission.[80] Copyright 2014, Royal Society of Chemistry

2.2 | Anthracite coal

Coal, especially anthracite with a high degree of coalification, contains many sp^2 microcrystals, which is easy to be exfoliated and surface modified by chemical oxidation. In order to rapidly separate these different-sized carbon domains, Ye and co-workers tuned the band gaps of anthracite coal-based GQDs (a-GQDs) in two ways: one was to change the pore size of cross-flow ultrafiltration membrane (Figure 3A), and the other was to control the chemical oxidation temperature directly.[83] In the first method, it was found that with the increase of corresponding hydrodynamic diameters from 10 ± 2.5 to 76 ± 18 nm, the average size of a-GQDs increased from 4.5 ± 1.2 to 70 ± 15 nm, and the QY of the obtained a-GQDs decreased from 1.1% to 0.38%. The study of photophysical properties of the separated a-GQDs showed that the maximum PL emission peak was redshifted from ~520 to ~620 nm, the a-GQDs solutions emitted light across the majority of the visible spectrum from green (~2.4 eV) to orange-red (~1.9 eV) regions, under 365 nm UV light irradiation. The relationship between the bandgap and a-GQDs size or molecular mass cutoff was summarized in Figure 3B. In the second method, the average size of a-GQDs decreased from 54 ± 7.2 to 7.6 ± 1.8 nm with the rise of oxidation temperature from 50 to 150°C in mixed acid (H_2SO_4 and HNO_3), and the temperature effect in bandgap engineering of a-GQDs was summarized in Figure 3C.

Meanwhile, Qiu's group reported the synthesis of anthracite coal-based CDs (a-CDs) with controllable structure by a combined technique of carbonization and HNO_3

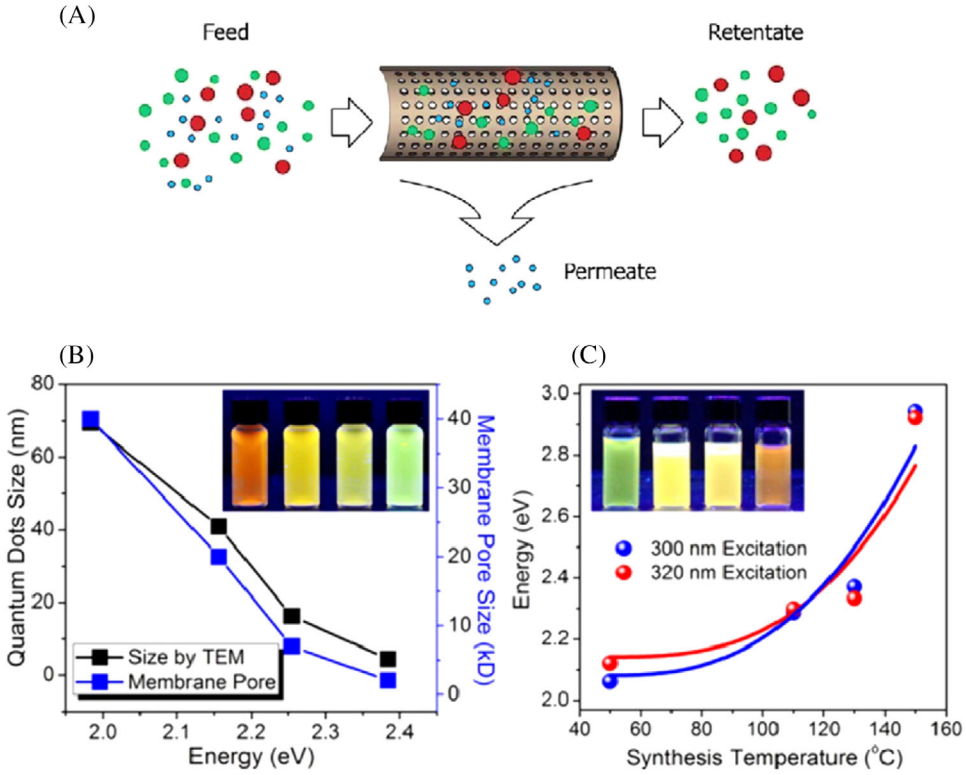

FIGURE 3 A, Schematic illustration of the separation of GQDs by cross-flow ultrafiltration; the relationship between energy bandgap and membrane pore size (B) and synthesis temperature (C). Reproduced with permission.[83] Copyright, 2015, American Chemical Society

oxidation.[84] The average size of a-CDs raised from 1.96 ± 0.73 to 3.10 ± 0.80 nm and the average height of a-CDs improved from 1.04 to 1.42 nm, when the carbonization temperature of anthracite coal increased from 0 to 1500°C. The nano-scale sp^2 carbon domains and surface defects resulted in two different emission modes (the short-wavelength emission at about 420 nm and long-wavelength emission at about 505 nm). In 2017, the same team reported the preparation of fluorescent nitrogen-doped CDs (N-CDs) from Taixi anthracite by a simple, green and sustainable one-pot solvothermal method in the presence of dimethylformamide (DMF).[85] The as-synthesized N-CDs emitted blue fluorescence at the excitation wavelength of 365 nm with singlet oxygen generation of 19% and QY of 47%, and the average size was 4.7 nm. Besides the complex and toxic strong acid oxidation method (e.g., HNO_3, H_2SO_4, hydrofluoric acid and potassium permanganate), Hu et al. had reported a simple, efficient and green method for the first time, to synthesize a-CDs with size distribution ranging from 1 to 3 nm.[86] This technique took the advantage of hydroxyl radicals (•OH) generated by the thermal excitation of H_2O_2 to attack the carbon atoms of nanoparticles containing hydroxyl and epoxy groups to form a-CDs (Figure 4A). It was found that long reaction time resulted in stronger fluorescence intensity (Figure 4B).

2.3 | Lignite

Thiyagarajan et al. applied ethylenediamine as both the reaction solvent and surface passivator to prepare structurally controllable and surface-functionalized carbon nanomaterials from lignite by reflux, microwave radiation, and laser ablation methods.[87] They found that the photoexcitation of the carbogenic nucleus (π-π^*) produced an electron-hole (e-h) pair, which relaxed and recombined at the diverse surface defect sites resulting in PL. The photophysical behavior could be observed only when the particle size was less than 10 nm. In 2017, Manoj's group reported the preparation of fluorescent organic semiconductor dots with adjustable particle size and surface function through chemical oxidation, followed by centrifugation, dialysis, and heating.[88] It was found that the lateral size of the nanocarbon fractions (Residue (LC1), the Supernatant (LC2), and the Permeate (LC3)) from lignite were 10–23, 10–17, ~5 nm, the thickness of them were 5–10, 4–8, 1–2 nm, and the I_D/I_G were 1.36, 0.72, 0.64, respectively. The maximum emission wavelength of LC1, LC2, and LC3 were 515, 517, 447 nm at the excitation wavelength of 440, 440, 320 nm. These nano fragments could be used to detect Cu^{2+} as low as 0.0089 nm in water. Later, the same group reported the fabrication of LC1C, LC2C, LC3C from LC1, LC2, and LC3 by chloroform ($CHCl_3$) reflux and

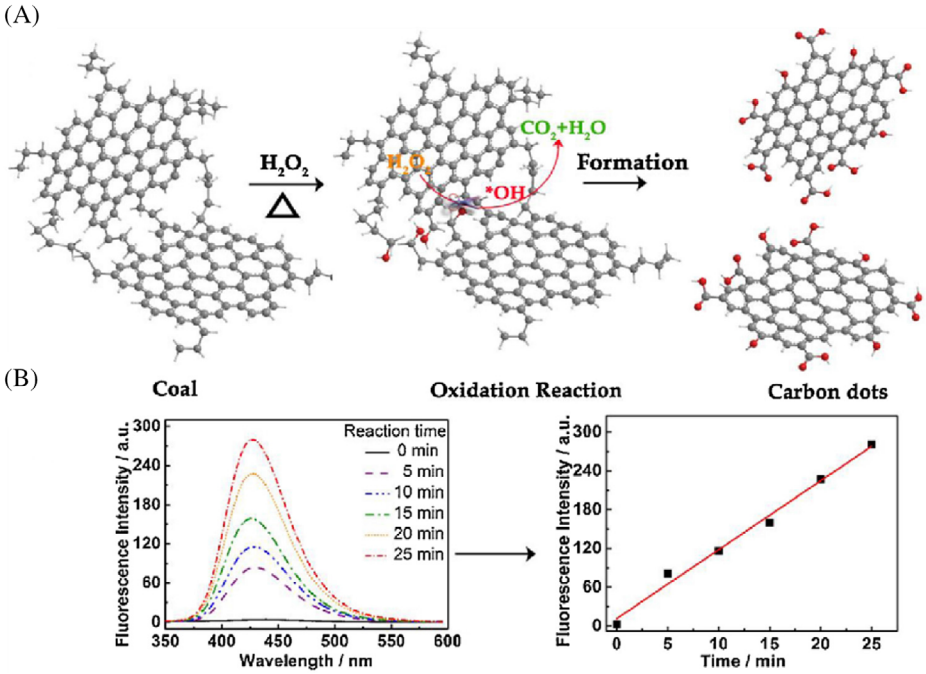

FIGURE 4 A, Schematic illustration of the forming of CDs. B, time-dependent fluorescence emission spectra of 2-hydroxyterephthalic acid formed by the reaction of terephthalic acid with •OH generated by reaction system under the heating at 80°C (left) and the time-dependent fluorescence intensities of 2-hydroxyterephthalic acid at 426 nm (right). Reproduced with permission.[86] Copyright 2016, Elsevier Ltd

direct oxidation with concentrated HNO_3.[89] They found that the band gaps of the LC1C, LC2C, LC3C were 2.90, 2.50, and 3.40 eV from the UV visible analysis by employing Tauc Plot. The size distribution of LC1C was 3–4 nm, the average size was 3.91 ± 0.32 nm, and the LC2C and LC3C nanostructures were stacking and agglomeration. With the improvement of excitation wavelength from 280 to 500 nm, the fluorescence spectra of all samples showed a redshift, and the maximum excitation wavelength of LC1C, LC2C, LC3C were 320, 340, 320 nm. The as-prepared carbon nanomaterials showed pH independence, which made them stable under any conditions. Liu et al. reported a green and facile fabrication method of CQDs from lignite adopting ozone as the oxidant to replace strong oxidizing acids.[90] It was found that the as-synthesized quantum dots had a yield of 35% with a size distribution of 2 to 4 nm. These quantum dots emitted strong blue fluorescence under 345 nm UV light irradiation and were able to detect Fe^{3+} as low as 0.26 μmol L^{-1}.

2.4 | Coal derivatives

In recent years, numerous researches have focused on preparing CDs from low-priced and abundant coal derivatives. Coal tar pitch (CTP), a side product of coking industry, has a unique molecule structure, consisting of an aromatic nucleus and multiple side chains bonding on this graphene-like nucleus, which is very similar to the structure of GQDs. Hu et al. prepared a multiple color and concentration-dependent CQDs from CTP powder in a mixture of formic acid and H_2O_2 without heating (Figure 5).[91] When the concentration of CDs decreased from 3.0 to 0.03 g L^{-1}, the fluorescence emission wavelength shifted to red. Under 365 nm excitation, the QY changed from 5.4% to 10.1%, which firstly increased and then decreased, and reached the maximum at 0.06 g L^{-1} (up to 10.1%). The yield of CDs was 49%. By contrast, the solid sample exhibited a wide absorption under UV visible light with the strongest absorption peak at around 440 nm and emitted bright red light under white light excitation. Liu and co-workers reported the preparation of GQDs with high solubility and strong fluorescence in aqueous solution from CTP by H_2O_2 oxidation under mild conditions (100°C for 2 hours in reflux).[92] The particle size distribution of GQDs-1 (15% H_2O_2 oxidation) and GQDs-2 (30% H_2O_2 oxidation) were 1.7 ± 0.4, 2.3 ± 0.7 nm, and the average thicknesses were 1–2, 1.9 ± 0.7 nm, respectively. Both GQDs-1 and GQDs-2 showed an excitation-dependent PL behavior. The yield and QY of CQDs-1 were 80% and 2.37%, and the optimum excitation and emission wavelengths were 325 and 445 nm. The as-synthetized CQDs emitted blue fluorescence under 325 nm excitation. Wang et al. reported the preparation of CQDs by direct carbonization of dispersed carbonaceous microcrystals from mesophase pitch (MP) without any strong oxidants (Figure 6).[93] With the rise of

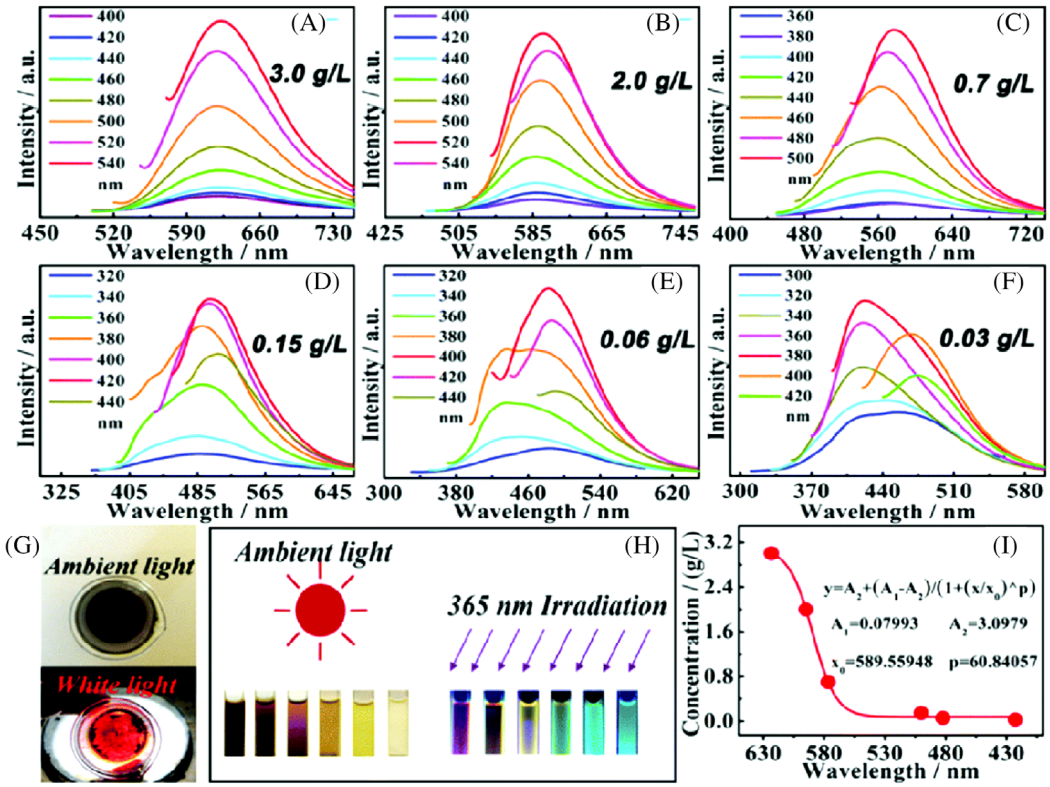

FIGURE 5 (A-F) PL spectra of the samples with different concentrations as labeled excited at different wavelengths. G, photos of solid CDs powders under ambient light and white light irradiation. H, photos of CDs solutions from 3.0–0.03 g L^{-1} under ambient light and 365 nm irradiation; and (I) the dependence of PL emission peaks on the concentrations of CDs. Reproduced with permission.[91] Copyright 2017, Royal Society of Chemistry

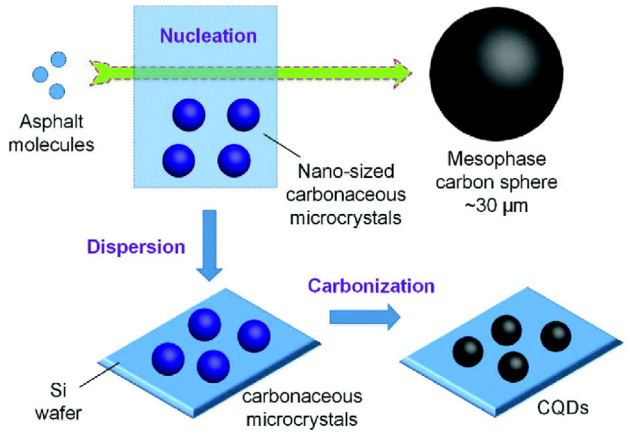

FIGURE 6 Schematic illustration of the fabrication of CQDs from MP. Reproduced with permission.[93] Copyright 2018, Royal Society of Chemistry

carbonization temperature from 430°C to 450°C, the particle size of CDs increased from 2.2 ± 0.37 to 4.5 ± 0.51 nm, the height improved from 2.0 to 4.5 nm, and the QY varied from 67% to 87%. CQD440 (carbonization temperature at 440°C) emitted a strong blue fluorescence when exposed to 365 nm UV light in ethanol, exhibited luminescence behavior independent of excitation, and there were three fixed emission peaks at 413, 435, and 460 nm.

Meanwhile, Zeng's group reported the preparation of the GQDs from coke by a one-step electrochemical stripping method (Figure 7).[94] By adjusting the current density and content of coke and water in the electrolyte solution, the structure of GQDs could be precisely adjusted to obtain multicolor fluorescent GQDs (green [G-GQDs], yellow [Y-GQDs], and orange [O-GQDs]). The yields of O-, Y-, G-, B-GQDs were 31.13%, 42.86%, 17.88%, 13.04% and the QYs of O-, Y-, G-, B-GQDs were 9.24%, 7.90%, 8.47%, 19.27%. The average size and height of O-, Y-, G-, B-GQDs were 4.61 ± 0.88, 4.15 ± 0.54, 3.02 ± 0.45, 2.90 ± 0.46, and 2.4, 2.0, 1.6, 1.3 nm, respectively. The maximum emission peaks appeared at 560, 530, 500, and 440 nm when O-, Y-, G- and B-GQDs aqueous solutions were excited at 470, 450, 380, and 340 nm wavelength. Also, the as-prepared G-GQDs could be further reduced by sodium borohydride to form new GQDs and emitted bright blue fluorescence (B-GQDs). Feng and Zhang had published an environmentally friendly and simple one-step chemical oxidation (H_2O_2) method to prepare fluorescent CQDs from coke for white light-emitting devices.[95] The QY of the as-produced CQDs was 9.2%, and the composition of the blue-green-red spectral was up to 48%. The obtained CQDs emitted blue fluorescence under 365 nm illumination and exhibited excitation-dependent PL emission

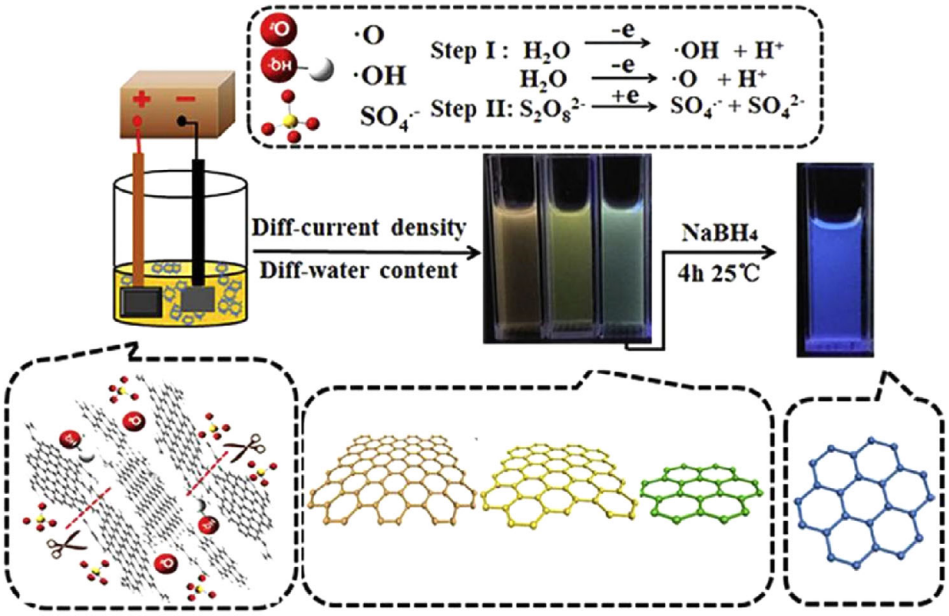

FIGURE 7 Schematic illustration of the synthetic process of multicolor GQDs from coke. Reproduced with permission.[94] Copyright 2018, Elsevier Ltd

behavior, with an average size of 6.5 nm. Geng et al. reported the preparation of CQDs from coal tar by a cost-effective solvothermal method (200°C for 12 hours in the toluene solution).[96] The as-made CQDs emitted strong and stable orange fluorescence at 605 nm excitation. The size of the CQDs was 1.5–4.5 nm, and the I_D/I_G was 1.029. The QY of the as-fabricated CQDs was 29.7% in toluene solution. After the modification of the liposomes, the CQDs became hydrophilic and showed a redshift of fluorescence to 640 nm under UV light. The QY of the liposome-CQDs was 10.7%, and lipsome-CQDs showed stable pH-independent behavior. Quinoline Insoluble (QI) residues existed in the form of solid carbon particles in coal tar. Kundu et al. reported the fabrication of high fluorescence CDs from the QI particles of coal tar by adding different oxidants in 2020.[97] The average size of the CD1 (H_2O_2 oxidation) and CD2 (H_2SO_4 and HNO_3 oxidation) were ~1 and ~5 nm, and the corresponding QY were 1% and 2%. The maximum excitation and emission wavelengths of CD1 were at 335 and 440 nm, and the utmost excitation and emission wavelengths of CD2 were at 490 and 578 nm.

3 | APPLICATIONS OF COAL-BASED CDS

3.1 | Energy-related applications

Ye and co-workers primarily assembled boron (B)- and nitrogen (N)-doped GQDs on graphene adopting a hydrothermal method (Figure 8A).[98] The as-fabricated hybrid material could be modified and applied for the catalyst by annealing at 1000°C for different time (10, 30, 60 minutes). These as-produced samples were denoted as N-GQD/G-30, BN-GQD/G-10, BN-GQD/G-30, N-GQD/G-60, and BN-G-30. Dopant-free GQD/G were annealed for 30 minutes as control samples and denoted as DF-GQD/G-30. The resulting hybrid material combined the advantages of the two materials, such as rich edges, doping sites, high conductivity (~11.0 mA cm^{-2}), and large superficial area, making it an excellent electrocatalyst for the oxygen reduction reaction (ORR). They found that the ORR activity was significantly affected by the doping time and dopant concentration. BN-GQD/G-30 exhibited the most positive initial potential and maximum current density in the whole potential range, possessed an almost complete four-electron ORR process (n = 3.93) and a large kinetic current (J_K = 11.1 mA cm^{-2}) (Figure 8B, C). The activity of the hybrid material (with ~15 mV more positive onset potential) in alkaline medium was even higher than commercial Pt/C. Zhang and co-workers had developed a template-assisted assembly method to fabricate the high performance hierarchical porous carbon nanosheets (HPCNs) for supercapacitor electrodes adopting coal-based GQDs as the building unit (Figure 9).[81] The obtained HPCNs showed an interconnected, loosely packed graphene-like structure, with a specific surface area of 1332 m^2 g^{-1}, well-organized pore distribution, good conductivity, rich active centers, and sufficient ion migration channels. Under the optimized conditions, the specific capacitance of HPCN-1:3 (0.5 g GQDs and 1.5 g magnesium hydroxide) was 200 F g^{-1} (1 A g^{-1}),

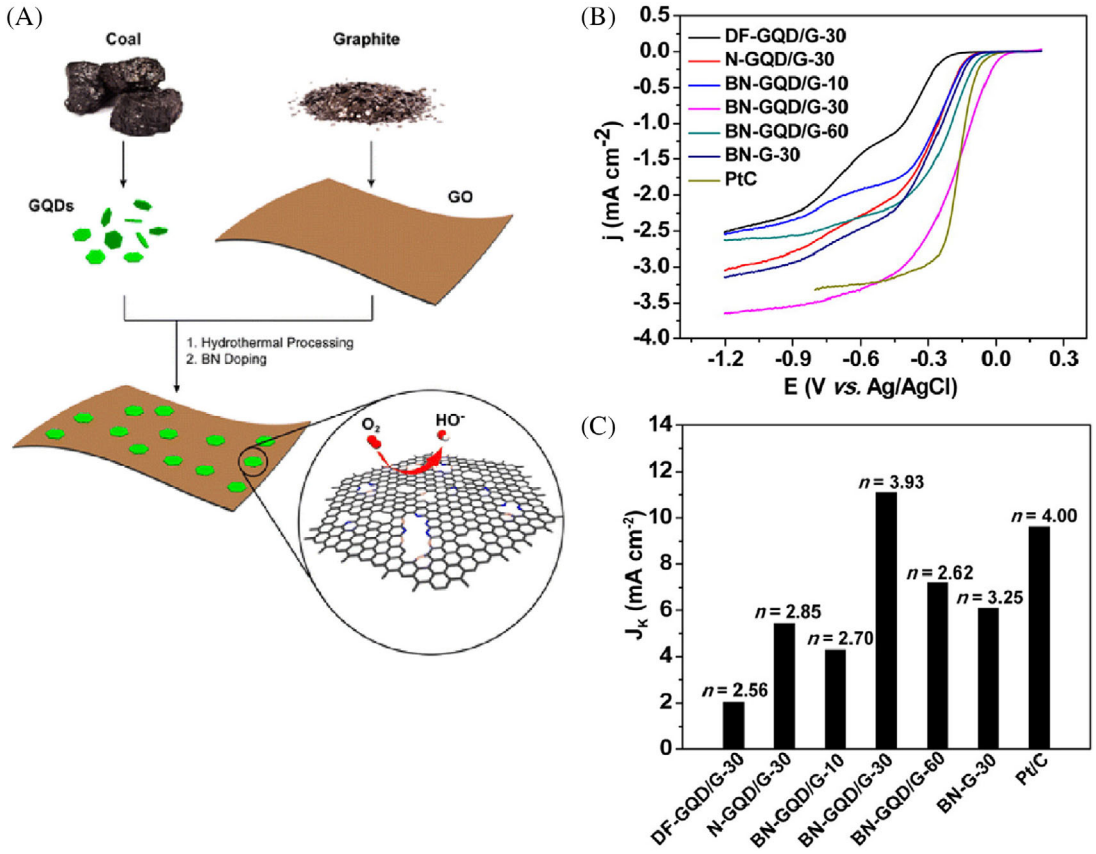

FIGURE 8 A, Schematic illustration of the preparation of the BN-GQD/G nanocomposite. B, rotating disk electrode linear sweep voltammograms of ORR. C, electrocatalytic activity of all samples in (B). Reproduced with permission.[98] Copyright, 2014, American Chemical Society

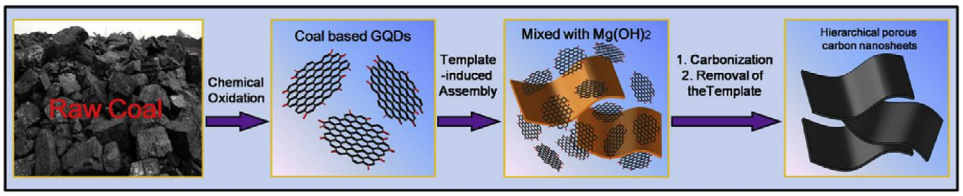

FIGURE 9 Schematic description for the preparation of the HPCNs. Reproduced with permission.[81] Copyright 2017, Elsevier Ltd

and the capacity remained at 112 F g^{-1} (100 A g^{-1}). A small amount of potassium hydroxide (KOH) was added for in-situ chemical activation in the preparation process, further improving its energy storage performance. AHPCN-1:0.25 (0.5 g GQDs and 0.125 g KOH) showed that the capacity improved to 230 F g^{-1} at 1 A g^{-1}, while the capacity remained at 170 F g^{-1} at 100 A g^{-1}, the capacitance retention rate was 74%. All samples showed excellent cycle stability, even after 10,000 cycles at 10 A g^{-1}, there was no obvious capacity degradation. This research indicated that GQDs were ideal precursors for the preparation of advanced energy storage materials. This technology was expected to open up new ways for the clean and efficient use of coal resources.

Wang et al. reported the preparation of graphene nanosheets (GNs) with outstanding stability and super capacity from inertinite and vitrinite rich coal. The capacitance and resistance of inertinite-based GNs were greater than those of vitrinite-based GNs.[99] Zhang et al. reported the preparation of coal-based GQDs/α-Fe_2O_3 nanocomposites with excellent cycling and rate capability by electrodeposition.[100] By adjusting the electrolytic solvent ratio (V_{DMF}:V_{Water} = 2:1), the antler-shaped α-Fe_2O_3 nanoparticles were prepared on a nickel substrate, and then GQDs/α-Fe_2O_3 composites were fabricated by two-step electrodeposition using GQDs solution as the electrolyte. The electrochemical test results demonstrated that the specific capacitance of GQDs/α-Fe_2O_3 composite could

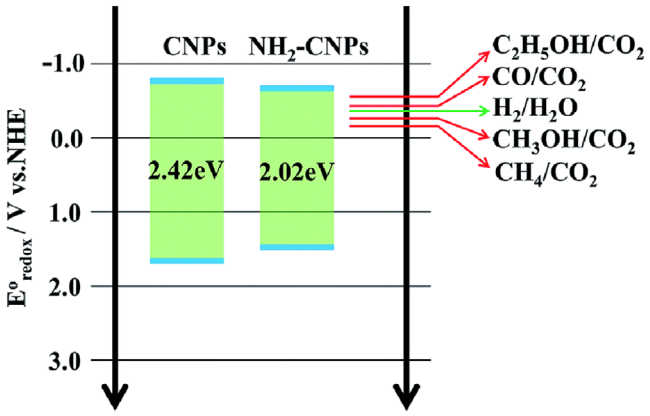

FIGURE 10 Schematic of the mechanism of the photocatalytic CO_2 reduction with water on NH_2-CNPs. Reproduced with permission.[102] Copyright 2018, Royal Society of Chemistry

reach 1582.5 mAh g^{-1} at the current density of 1A g^{-1}. After 110 cycles, the charge-discharge specific capacitance was still as high as 1320 mAh g^{-1}, indicating that the cycle performance had been improved. In addition, the specific capacity of GQDs/α-Fe_2O_3 composite could reach 1091 mAh g^{-1} at high current density (5 A g^{-1}), which exhibited its ideal rate performance.

3.2 | Environment-related applications

3.2.1 | Catalytic applications

At present, the best way to solve the problem of increasing carbon dioxide (CO_2) emissions and energy shortage is to use solar radiation to reduce CO_2 into organic fuels catalytically. Maimaiti's group reported CDs/TiO_2 nanoparticles' preparation with a diameter of 30–50 nm.[101] They found that the CDs/TiO_2 nanoparticles connected with C = C, C-OH/C-O-C, C = O, Ti-O and other functional groups, and the bandgap decreased from 3.2 eV of pure TiO_2 to 2.9 eV of the as-prepared CDs/TiO_2. The removal rate of COD_{Cr} was 81.2%, and most organic compounds (except nitrogen heterocyclic compounds) in the black liquor were degraded after 3 hours of treatment. They synthesized N, S co-doped ammoniated coal-based carbon nanoparticles (NH_2-CNPs) via thionyl chloride chlorination and ethylenediamine passivation.[102] The bandgap of NH_2-CNPs reduced from 2.42 eV of CNPs to 2.02 eV, and the products of CO_2/H_2O_2 photocatalytic reduction by NH_2-CNPs were methanol (CH_3OH), carbon monoxide (CO), ethanol (C_2H_5OH), hydrogen (H_2) and methane (CH_4) (Figure 10). The total amount of products was 807.56 μmol g^{-1} cat., and the content of CH_3OH was 618.7 μmol g^{-1} cat. after reaction for 10 hours. The same group also fabricated a cuprous oxide (Cu_2O)-based composite photocatalyst composed of Cu_2O/CNPs.[103] The physical properties, chemical structure of Cu_2O/CNPs and the photocatalytic activity of CO_2/H_2O reduction to CH_3OH were studied. The studies showed that the Cu_2O/CNPs were consisted of spherical particles with a diameter of 50 nm, had a mesoporous structure, and were suitable for CO_2 adsorption. Under visible light irradiation, e-h pairs were generated in Cu_2O. Because of the presence of CNPs, the rapid recombination of e-h pairs was inhibited. The energy gradient formed on the Cu_2O/CNPs surface facilitated the effective separation of e-h pairs during CO_2 reduction and H_2O oxidation, leading to improved photocatalytic activity. Optimizing the loading amount of CNPs was the key to the activity of the Cu_2O photocatalyst. When the loading of CNPs was 73.12%, the yield of CH_3OH was 169.40 μmol g^{-1} cat. after 12 hours. The yield of CH_3OH in the fifth cycle of the photocatalyst was still 90.6% of the initial yield, indicating that the photocatalyst's stability and reusability were excellent. Meanwhile, they prepared Ag/CDs composite nanoparticles by adopting a simple silver mirror reaction to attach CDs to the silver surface in situ.[104] The composite material's surface contained a large number of oxygen groups and a mesoporous interface formed by the accumulation of uniform particles, which were advantageous to a good adsorption capacity for CO_2. Within the measurement range, Ag/CDs containing 16% of CDs exhibited the highest catalytic activity. After 10 hours of light, the yield of CH_3OH from photocatalytic CO_2 reduction reached 17.82 μmol, which was almost three times higher than that of pure Ag catalyst.

Recently, Liu and co-workers had successfully prepared an efficient, reusable and stable CTP/TiO_2 composite photocatalyst from CTP by a simple and environmental friendly one-step solvothermal method (Figure 11).[105] The CTP/TiO_2 nanocomposites had a relatively uniform shape with an average size of 5.17 ± 0.95 nm, the degradation efficiency of CTP/TiO_2 nanocomposites increased from 41.0% to 91.1% with the content of CTP varied from 1% to 5%, and the photocatalytic degradation rate of CTP/TiO_2 nanocomposites was 23 times higher than that of pure TiO_2 at the optimum content of CTP. The possible chemical reactions during the degradation of Rhodamine B (RhB) were as follows:

$$\mathrm{CTP/TiO_2} + h\nu \rightarrow e^- + h^+ \quad (1)$$

$$\mathrm{H_2O} + h^+ \rightarrow H^+ + \cdot OH \quad (2)$$

$$\mathrm{O_2} + e^- \rightarrow \cdot O_2^- \quad (3)$$

$$\cdot O_2^- + 2H^+ + e^- \rightarrow \mathrm{H_2O_2} \quad (4)$$

$$\mathrm{H_2O_2} + e^- \rightarrow \cdot OH + OH^- \quad (5)$$

FIGURE 11 Schematic illustration of the preparation of CTP/TiO_2 composite photocatalysts by a one-step solvothermal reaction. Reproduced with permission.[105] Copyright 2019, Elsevier Ltd

$$H_2O \rightarrow H^+ + OH^- \quad (6)$$

$$OH^- + h^+ \rightarrow \cdot OH \quad (7)$$

$$\cdot OH + RhB \rightarrow CO_2 + H_2O \quad (8)$$

$$\cdot O_2^- + RhB \rightarrow CO_2 + H_2O \quad (9)$$

Different from other coal-based CQDs, lignite-derived CQDs showed obvious concentration-dependent red-shifted absorption, remarkable aggregation-induced diverse color emissions and intense orange-red solid-phase fluorescence. Yu et al. synthesized the CQDs/TiO_2 nanocomposites by an in situ method.[106] According to optimize the loading ratio of CQDs, they found that CQDs/TiO_2 containing 2 wt.% of CQDs exhibited the best photocatalytic degradation of RhB (close to 95%) under visible light. The photoelectrochemical characterization of CQDs/TiO_2 confirmed that the improvement of CQDs/TiO_2 photocatalytic performance was due to the heterostructure interface between CQDs and TiO_2, which reduced the bandgap of TiO_2, changed the absorption boundary, and significantly accelerated electrons and holes. The separation of holes made CQDS become electron donors, providing more electrons for the photocatalytic process.

3.2.2 | Sensing applications

The coal-based CDs exhibit low toxicity and significant fluorescence characteristics, which can be applied as a probe for ion detection in environmental protection and biological analysis. Qiu's group reported that the CDs reduced by sodium borohydride (r-CDs) was an effective fluorescence sensing material, which could detect Cu^{2+} with a detection limit of 2.0 nM.[84] It was found that Cu^{2+} exhibited the highest selectivity for the fluorescence quenching of r-CDs. In contrast, this selectivity hardly changed in the presence of other metal ions. In 2019, Zhang et al. fabricated a-CQDs with uniform size distribution and a diameter of 3.2 ± 1.0 nm by ultrasonic physical cutting method, which also could be used to detect Cu^{2+}.[107] Xu and co-workers reported that the N, P, and S co-doped coal-based CDs could detect Pb^{2+} as low as 0.75 μM, with a linear dynamic range of 1–20 μM.[108] Hu et al. synthesized CDs with dual PL peaks adopting diammonium phosphate as a modifier, which could be used to determine the pH distribution and change in complex systems containing interfering metal ions.[109] Manoj's group reported the preparation of pH-independent CDs from lignite, an unlabeled and effective probe for selective detection of glucose ions with a detection limit of 0.125 mM.[89]

3.3 | Biomedical applications

To estimate whether liposome-CQDs could be used as biological probes, Geng et al. studied the evolution of liposome-CQDs activity in 24 and 48 hours at doses of 20, 40, 60, 80 and 100 mg L^{-1} adopting HeLa cells as the model (Figure 12).[96] After injection of these solutions, the cytoplasm showed enhanced fluorescence around the nucleus. The excitation wavelengths of the confocal microscopic images were 405, 488, and 546 nm, and the detection wavelengths were in the range of 420–480, 505–540, and 550–620 nm (Figure 12A-D). By taking tumor-bearing nude mice as an animal model, they found that the strong fluorescence signals (emission wavelength at 620 nm) could be clearly observed in the tumor area where liposome-CQDs were injected at 580 nm excitation after 0.5 hours of injection (Figure 12E). The liposome-CQDs accumulated in the tumor area, and the obvious fluorescence could be observed compared with other tissues after 1 hours of injection (Figure 12F). When the imaging dose was 40 mg L^{-1}, the cell survival rate remained above 92% after 24 hours of incubation, and there was no obvious cytotoxicity at low doses (Figure 12G). The research demonstrated that the fluorescent liposome-CQDs exhibited good biocompatibility and was suitable for the biomedical field. It could be used as an excellent in vitro and in vivo imaging marker materials. Meanwhile, Wang and Co-Workers reported a

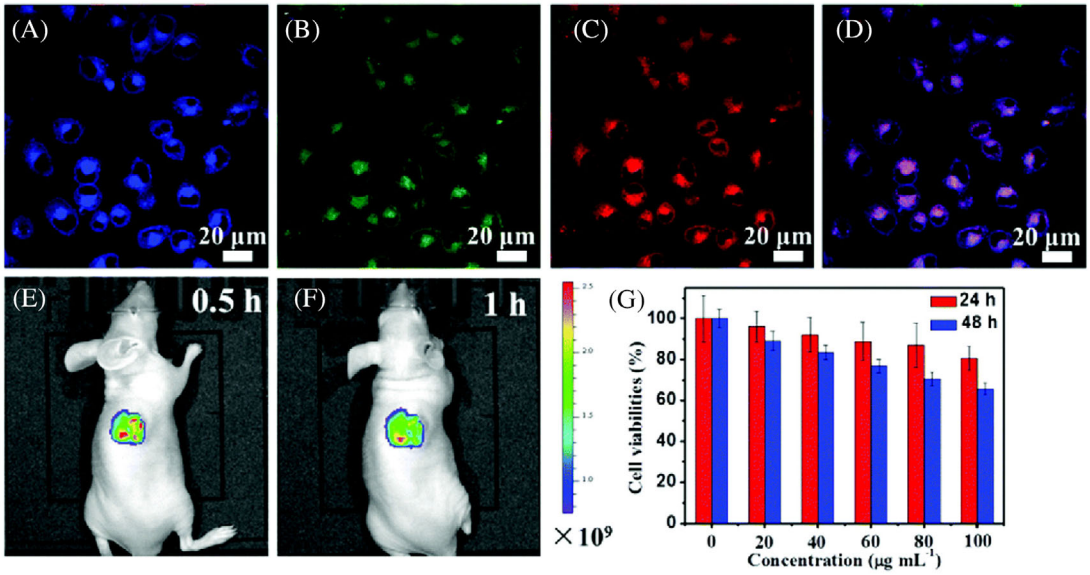

FIGURE 12 Confocal fluorescence image at 405, 488, and 546 nm excitation (A-C) and merge image (D) of HeLa cells using liposome-CQDs internalized into the cytoplasm of the cells; (E and F) in vivo fluorescence images of HeLa tumor-bearing nude mice obtained in tumor sites at 0.5 and 1 hour after intratumor injection of 200 μL of an aqueous solution of liposome-CQDs. The color bars represent the fluorescence intensity. G, cytotoxicity assessment of liposome-CQDs at higher doses for incubation time varied from 24 to 48 hours using HeLa cells. Reproduced with permission.[96] Copyright 2017, Royal Society of Chemistry

one-pot hydrothermal method for synthesizing amine and sulfur-based co-functional GQDs.[110] It was found that the as-synthesized GQDs showed super stability and attractive two-photon fluorescence properties. The as-produced GQDs had a two-photon absorption cross-section of 31000 GM, which greatly exceeded most conventional fluorescent materials. Non-cytotoxic GQDs exhibited negligible photothermal effects under 808 nm femtosecond laser irradiation, suitable for the long-term two-photon imaging and observation. These findings opened up new possibilities for the applications of the two-photon fluorescent GQDs in various biological fields.

Kang et al. firstly developed a green and facile pulsed laser ablation in liquid to prepare graphene oxide quantum dots (GOQDs) with excellent optical properties from the abundant and low-cost coal.[111] They found that the pancreas cancer cells (PanC-1) effectively retained the original morphology after incubation with GOQDs, and showed a green PL. When the GOQD concentration increased from 0.1 to 5 mg mL^{-1}, the PanC-1 cell survival rate was still more than 85%, indicating that the unmodified GOQDs with low toxicity and good biocompatibility was a kind of promising biological imaging material. Furthermore, some researchers take interests in developing antioxidants that can treat diseases associated with excessive oxidative stress, and the efficacy is comparable to that of metalloenzymes. Nilewski and co-workers,[112] reported the preparation of coal-derived GQDs and their polyethylene glycol (PEG) functionalized derivatives as effective antioxidants (Figure 13A). It was found that the onset voltage of aGQDs and bGODs were close to −0.2 V, covering a wide range with a maximum peak at −1.5 V, demonstrating that the antioxidants of aGQDs and bGQDs were stronger than GO. According to the initial peak potential, the as-fabricated antioxidants' strength was almost the same as that of the hydrophilic carbon clusters (HCCs) (Figure 13B). Compared with bGQDs, aGQDs protected more cells at a lower concentration, and the data were as follows: aGQD versus bGQD (2 mg L^{-1}): 87.1 ± 18.3 versus 75.7 ± 11.62, $P = .042$; aGQD versus bGQD (4 mg L^{-1}): 104.5 ± 14.8 versus 77.7 ± 12.1, $P < .0001$; aGQD versus bGQD (8 mg L^{-1}): 102.2 ± 11.1 versus 88.8 ± 9.6, $P = .0079$ (Figure 13C, D). Recently, Ghorai et al. reported that GQDs were internalized into the cell-matrix and nucleus of breast cancer cells, which could effectively introduce chemotherapeutic drugs into specific tumor targeting sites, and exhibited great potential applications in tumor treatment.[79]

3.4 | Applications in polymer composites

Owing to a large number of polar functional groups, coal-based GQDs can be applied in polymer composites without any surface modification. Kovalchuk et al. used polyvinyl alcohol (PVA) as the matrix polymer and GQDs as the raw material to prepare the luminescent polymer PVA/GQDs nanocomposite by the casting method.[113] They found that the as-fabricated composite films achieved high optical

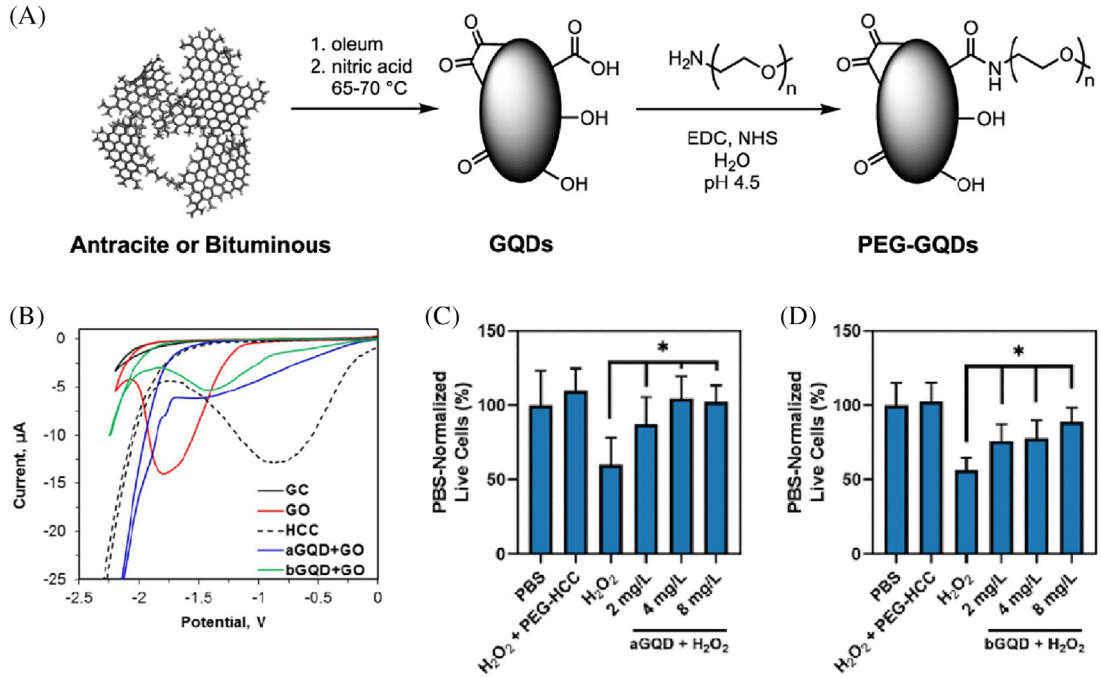

FIGURE 13 A, Schematic illustration of PEG-GQDs from coal. B, CV of GO, HCCs, aGQDs + GO, and bGQDs + GO. (C) and (D) cell viability following different treatments. Reproduced with permission.[112] Copyright, 2019, American Chemical Society

transparency (78-91%), and the nanoparticles showed good dispersibility under the GQDs concentration of 1%–5% in the PVA. The composite material exhibited a concentration dependence. With the improvement of GQDs content, the PL intensity gradually increased. When the GQDs content was 10%, the material's PL intensity reached the largest (Figure 14). These obtained PVA/GQDs nanocomposites had a wide PL emission spectrum, covering most of the visible light range, which could be utilized in light-emitting diodes (LEDs), flexible electronic displays, and other optoelectronic applications.

Polyacrylonitrile electrospun carbon nanofiber fabrics (ECNFs) are considered to be provided with great potential in many fields. However, the finite strength and flexibility greatly hinder their practical applications without optimization. Zhu et al. reported the preparation of tough, flexible and hydrophobic ECNFs by crosslinking coal-based GQDs (Figure 15A).[114] It was found that the strength, flexibility, and hydrophobicity of ECNFs were significantly improved by simply adding coal-based GQDs to the spinning solution. As the content of coal-based GQDs increased, the hydrophobicity of ECNFs gradually improved. ECNF-1.0 (0.4 g GQDs and 0.4 g ECNFs) showed the best hydrophobicity and super lipophilicity (Figure 15B). The ECNFs with coal-based GQDs exhibited outstanding strength and flexibility and could be twisted or folded into other shapes. After unfolding, the fabric could be restored to its original state without any cracks (Figure 15C, D). However, the ECNF-0 derived from the

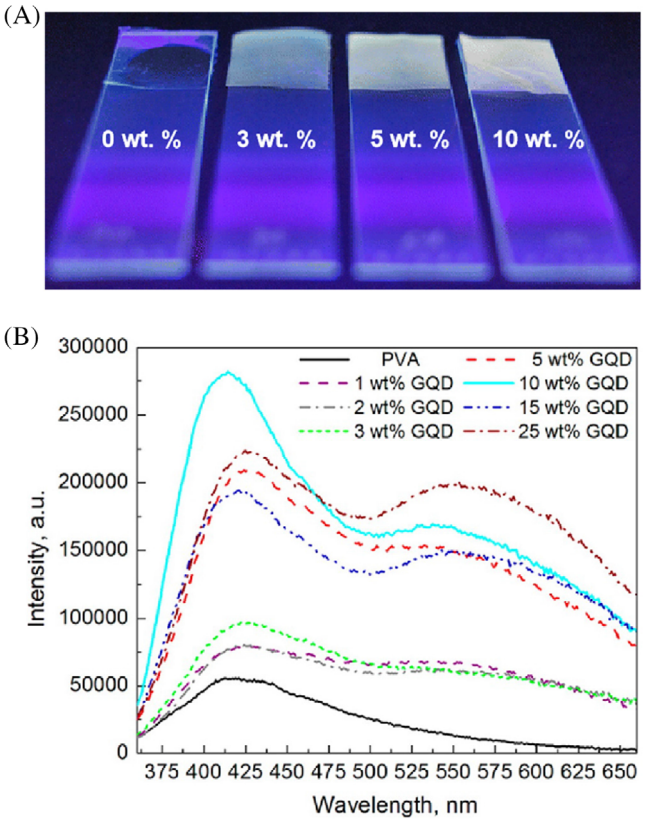

FIGURE 14 Photograph (A), PL spectra (B) of the PVA and PVA/GQD composite films. Reproduced with permission.[113] Copyright 2015, American Chemical Society

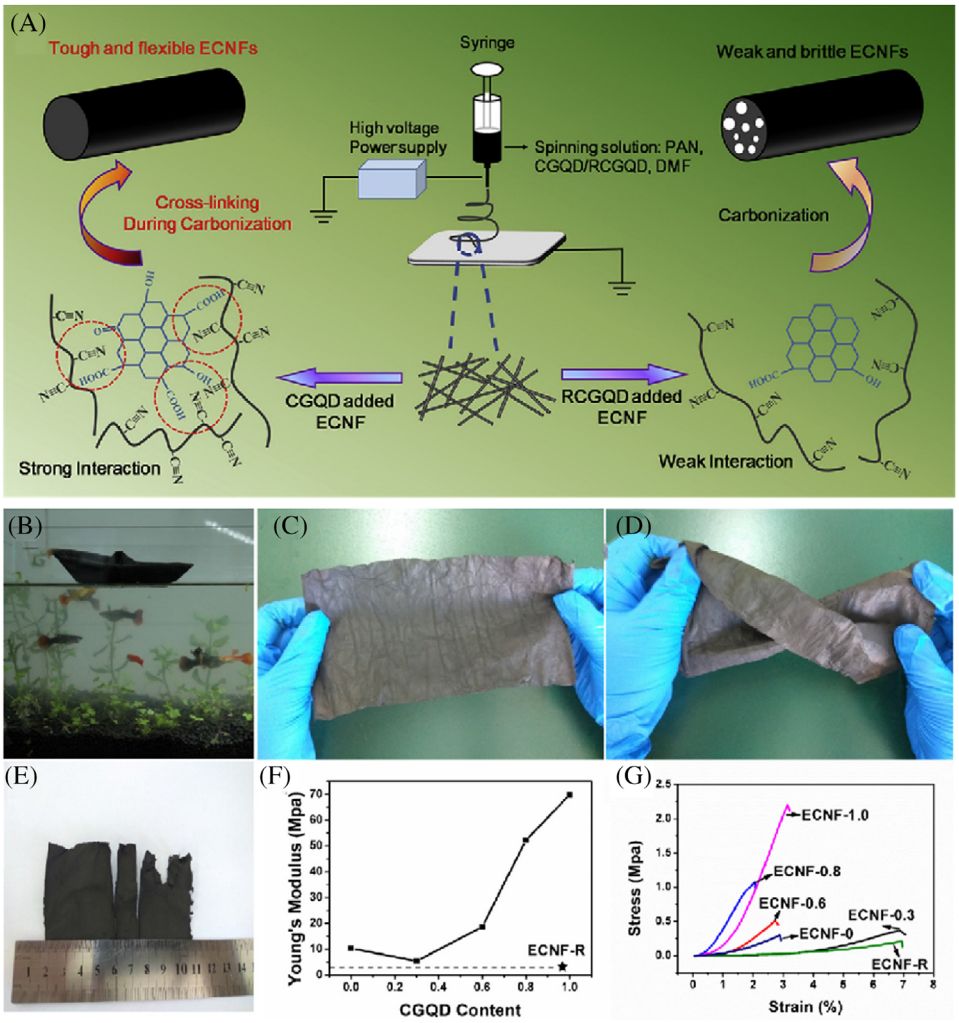

FIGURE 15 A, Schematic of the ECNF preparation procedure. B, ECNF-1.0 paperboat. C, before and (D) after being twisted. E, photograph of ECNF-0 after slight compression. F, the Young's modulus and (G) the stress-strain curves of the ECNFs. Reproduced with permission.[114] Copyright 2017, Elsevier Ltd

pure polyacrylonitrile (PAN) displayed special fragile (Figure 15E). The maximum tensile stress of ECNF-1.0 was about 2.2 Mpa, and the Young's modulus was about 70 MPa (Figure 15F, G).

4 | CONCLUSIONS, PROSPECTS, AND CHALLENGES

In this article, we reviewed the latest progress of coal-based CDs synthesis and their potential applications in the fields of energy, environment, biomedical, and polymer composites fields. There is an obvious trend that researchers are drawing more attention on the preparation of CDs from inexpensive and abundant coal derivatives (coke, coal pitch, coal tar, etc.) by green, simple, and efficient methods. In particular, H_2O_2 chemical oxidation represents a promising, environmentally friendly and safe way for the massive preparation of CDs. By adjusting the band gaps and heteroatom (N, P, S, and B) doping, the electroluminescence, photoluminescence and absorption characteristics of CQDs/GQDs can be effectively controlled, owing to their quantum confinement effect and edge effect. The ability to produce coal-based CDs on a large scale can significantly contribute to the long-term feasibility development of the applications mentioned above, and commercialize the green and cost-effective CDs, which will benefit people's lives. Making full use of these new nanomaterials, the research of CDs has quickly become the focus of people's attention. To this end, several knowledge gaps need to be resolved: (1) To further understand the relationship between the structure and properties of CDs, such as the influence of the shape, functional groups, and defects of CDs on the properties. (2) To further develop an environmentally friendly, safe, efficient, and industrially feasible synthetic method of CDs and improve CDs' yield and QY.

(3) Deepening the mechanism of coal-based CDs in related application fields and exploring potential application possibilities in other areas.

ACKNOWLEDGMENTS

This work is supported by National Natural Science Foundation of China (21976002, 22004003, 21675158 and 61603001) and Anhui Provincial Natural Science Foundation for Distinguished Young Scholars (2008085J11).

ORCID

Kui Zhang https://orcid.org/0000-0002-5634-9952

REFERENCES

1. S. Vasireddy, B. Morreale, A. Cugini, C. Song, J. J. Spivey, *Energy Environ. Sci.* **2011**, *4*, 311.
2. J. P. Mathews, A. L. Chaffee, *Fuel* **2012**, *96*, 1.
3. S. Iijima, *Nature* **1991**, *354*, 56.
4. K. Moothi, S. E. Iyuke, M. Meyyappan, R. Falcon, *Carbon* **2012**, *50*, 2679.
5. T. K. Zhang, Q. Wang, G. Q. Li, Y. Q. Zhao, X. M. Lv, Y. H. Luo, Y. F. Zhang, *Fuel* **2019**, *239*, 230.
6. I. Camean, P. Lavela, J. L. Tirado, A. B. Garcia, *Fuel* **2010**, *89*, 986.
7. X. Mu, Z. Q. Xu, Y. H. Xie, H. Y. Mi, J. H. Ma, *J. Alloys Compd.* **2017**, *711*, 374.
8. H. Y. Zhao, L. X. Wang, D. Z. Jia, W. Xia, J. Li, Z. P. Guo, *J. Mater. Chem. A* **2014**, *2*, 9338.
9. T. Das, P. K. Boruah, M. R. Das, B. K. Saikia, *RSC Adv.* **2016**, *65*, 39359.
10. K. S. Novoselov, A. K. Geim, S. V. Morozov, D. Jiang, S. V. Dubonos, I. V. Grigorieva, A. A. Frisov, *Science* **2004**, *306*, 666.
11. S. Awasthi, K. Awasthi, A. K. Ghosh, S. K. Srivastava, O. N. Srivastava, *Fuel* **2015**, *147*, 35.
12. X. Y. Xu, R. Ray, Y. L. Gu, H. J. Ploehn, L. Gearheart, K. Raker, W. A. Scrivens, *J. Am. Chem. Soc.* **2015**, *126*, 12736.
13. Y. P. Sun, B. Zhou, Y. Lin, W. Wang, K. A. S. Fernando, P. Pathak, M. J. Meziani, B. A. Harruff, X. Wang, H. F. Wang, P. G. Luo, H. Yang, M. E. Kose, B. Chen, L. M. Veca, S. Y. Xie, *J. Am. Chem. Soc.* **2006**, *128*, 7756.
14. C. L. Xia, S. J. Zhu, T. L. Feng, M. X. Yang, B. Yang, *Adv. Sci.* **2019**, *6*, 1.
15. G. E. Lecroy, S. K. Sonkar, F. Yang, L. M. Veca, P. Wang, K. N. Tackett, J. J. Yu, E. Vasile, H. Qian, Y. Liu, *ACS Nano* **2014**, *8*, 4522.
16. P. Anilkumar, L. Cao, J. Yu, K. N. Tackett, P. Wang, M. J. Meziani, Y. Sun, *Small* **2000**, *4*, 545.
17. J. H. Shen, Y. H. Zhu, X. L. Yang, C. Z. Li, *Chem. Comm.* **2012**, *48*, 3686.
18. Y. Q. Feng, J. P. Zhao, X. B. Yan, F. L. Tang, Q. J. Xue, *Carbon* **2014**, *66*, 334.
19. M. J. Krysmann, A. Kelarakis, P. Dallas, E. P. Giannelis, *J. Am. Chem. Soc.* **2011**, *134*, 747.
20. R. Wang, K. Q. Lu, Z. R. Tang, Y. J. Xu, *J. Mater. Chem. A* **2017**, *5*, 3717.
21. Y. F. Wang, A. G. Hu, *J. Mater. Chem. C* **2014**, *2*, 6921.
22. L. B. Li, D. Tao, *J. Mater. Chem. C* **2018**, *6*, 7944.
23. D. Deepa, T. Bhattacharya, B. Majumdar, S. Mandani, T. Sarma, *Dalton Trans.* **2013**, *42*, 13821.
24. C. Y. Li, Y. H. Zhu, X. Q. Zhang, X. L. Yang, C. Z. Li, *RSC Adv.* **2012**, *2*, 1765.
25. H. Z. Zheng, Q. L. Wang, Y. J. Long, H. J. Zhang, X. X. Huang, R. Zhu, *Chem. Comm.* **2011**, *47*(38), 10650.
26. S. H. Miao, K. Liang, J. J. Zhu, B. Yang, B. Kong, *Nano Today* **2020**, *33*, 100879.
27. M. Han, S. J. Zhu, Y. B. Song, T. L. Feng, S. Y. Tao, J. J. Liu, B. Yang, *Nano Today* **2018**, *19*, 201.
28. J. Briscoe, A. Marinovic, M. Sevilla, S. Dunn, T. Magdalena, *Angew. Chem. Int. Ed.* **2015**, *54*, 4463.
29. R. Sekiya, Y. Uemura, H. Murakami, T. Hai, *Angew. Chem. Int. Ed.* **2014**, *126*, 5725.
30. H. R. Jia, Z. B. Wang, T. Yuan, F. L. Yuan, X. H. Li, Y. C. Li, Z. A. Tan, L. Z. Fan, S. H. Yang, *Adv. Sci.* **2019**, *6*, 1900397.
31. S. J. Zhu, J. H. Zhang, S. J. Tang, C. Y. Qiao, L. Wang, H. Y. Wang, X. Liu, B. Li, Y. F. Li, W. L. Yu, X. F. Wang, H. C. Sun, B. Yang, *Adv. Funct. Mater.* **2012**, *22*, 473.
32. M. Zheng, Z. G. Xie, D. Qu, D. Li, P. Du, X. B. Jing, Z. C. Sun, *ACS Appl. Mater. Interfaces* **2013**, *5*, 13242.
33. H. Zhu, X. L. Wang, Y. L. Li, Z. J. Wang, F. Yang, X. R. Yang, *Chem. Comm.* **2009**, *1*, 5118.
34. B. R. Diego, J. C. Canga, J. C. Mayo, R. M. Sainz, J. R. Encinar, M. C. F. Jose, *Adv. Funct. Mater.* **2019**, *29*, 1903884.
35. P. H. Zhao, M. L. Yang, W. Y. Fan, X. J. Wang, F. L. Tang, C. P. Yang, X. W. Dou, S. Y. Li, Y. N. Wang, Y. W. Cao, *Part. Part. Syst. Cha.* **2016**, *33*, 635.
36. Y. Xu, M. Wu, Y. Liu, X. Z. Feng, X. B. Yin, X. W. He, Y. K. Zhang, *Chem. Eur. J.* **2013**, *19*, 2276.
37. S. Sarkar, K. Das, M. Ghosh, P. K. Das, *RSC Adv.* **2015**, *5*, 65913.
38. S. Chandra, P. Das, S. Bag, D. Laha, P. Pramanik, *Nanoscale* **2011**, *4*, 1533.
39. Z. Yang, M. H. Xu, Y. Liu, F. J. He, F. Gao, Y. J. Su, Y. F. Zhang, *Nanoscale* **2014**, *6*, 1890.
40. R. Z. Zhang, W. Chen, *Biosens. Bioelectron.* **2014**, *55*, 83.
41. Y. P. Sun, C. Shen, J. Wang, Y. Lu, *RSC Adv.* **2015**, *5*, 16368.
42. Q. Xu, P. Pu, J. G. Zhao, C. B. Dong, C. Gao, Y. S. Chen, J. R. Chen, Y. Liu, H. J. Zhou, *J. Mater. Chem. A* **2015**, *3*, 542.
43. W. J. Lu, X. J. Gong, M. Nan, Y. Liu, S. M. Shuang, C. Dong, *Anal. Chim. Acta* **2015**, *898*, 116.
44. S. L. Hu, R. X. Tian, Y. G. Dong, J. L. Yang, J. Liu, Q. Chang, *Nanoscale* **2013**, *5*, 11665.
45. H. T. Li, X. D. He, Z. H. Kang, H. Huang, Y. Liu, J. L. Liu, S. Y. Lian, C. H. A. Tsang, X. B. Yang, S. T. Lee, *Angew. Chem. Int. Ed.* **2010**, *122*, 4532.
46. M. K. Barman, B. Jana, S. Bhattacharyya, A. Patra, *J. Phys. Chem. C* **2014**, *118*, 20034.
47. A. Jaiswal, P. K. Gautam, S. S. Ghosh, A. Chattopadhyay, *J. Nanopart. Res.* **2014**, *16* (1) 2188.
48. F. Wang, Y. H. Chen, C. Y. Liu, D. G. Ma, *Chem. Comm.* **2011**, *47*, 3502.
49. W. Kwon, Y. H. Kim, C. L. Lee, M. Lee, H. C. Choi, T. W. Lee, S. W. Rhee, *Nano Lett.* **2014**, *14*, 1306.
50. L. P. Huang, B. Wu, J. Y. Chen, Y. Z. Xue, Y. M. Li, *Carbon* **2011**, *49*, 4792.
51. X. Guo, C. F. Wang, Z. Y. Yu, C. Li, S. Chen, *Chem. Comm.* **2012**, *48*, 2692.

52. S. W. Yang, J. Sun, X. B. Li, W. Zhou, Z. Y. Wang, P. He, G. Q. Ding, X. M. Xie, Z. H. Kang, M. H. Jiang, *J. Mater. Chem. A* **2014**, *2*, 8660.
53. A. B. Bourlinos, A. Stassinopoulos, D. Anglos, R. Zboril, *Small* **2008**, *4*, 455.
54. L. Cao, X. Wang, M. J. Meziani, F. S. Lu, H. F. Wang, P. G. Luo, Y. Lin, B. A. Harruff, L. M. Veca, D. Murray, *J. Am. Chem. Soc.* **2007**, *129*, 1318.
55. L. Bao, Z. L. Zhang, Z. Q. Tian, L. Zhang, C. Liu, Y. Lin, B. P. Qi, D. W. Pang, *Adv. Mater.* **2011**, *23*, 5801.
56. S. J. Zhu, Q. N. Meng, L. Wang, J. H. Zhang, Y. B. Song, H. Jin, K. Zhang, H. C. Sun, H. Y. Wang, B. Yang, *Angew. Chem. Int. Ed.* **2013**, *125*, 4045.
57. J. Peng, W. Gao, B. K. Gupta, Z. Liu, R. A. Romero, L. H. Ge, L. Song, L. B. Alemany, X. B. Zhan, G. H. Gao, S. A. Vithayathil, B. A. Kaipparettu, A. A. Marti, T. Hayashi, J. J. Zhu, P. M. Ajayan, *Nano Lett.* **2012**, *12*, 844.
58. K. Jiang, S. Sun, L. Zhang, Y. Lu, A. G. Wu, C. Z. Cai, H. W. Lin, *Angew. Chem. Int. Ed.* **2015**, *127*, 5450.
59. J. Lu, J. X. Yang, J. Z. Wang, A. Lim, S. Wang, K. P. Loh, *ACS Nano* **2009**, *3*, 2367.
60. L. L. Li, G. H. Wu, G. H. Yang, J. Peng, J. W. Zhao, J. J. Zhu, *Nanoscale* **2013**, *5*, 4015.
61. F. Liu, M. H. Jang, H. D. Ha, J. H. Kim, Y. H. Cho, T. S. Seo, *Adv. Mater.* **2013**, *25*, 3657.
62. S. M. Ardekani, A. Dehghani, M. Hassan, M. Kianinia, I. Aharonovich, V. G. Gomes, *Chem. Eng. J.* **2017**, *330*, 651.
63. E. Haque, S. Sarkar, M. Hassan, M. S. Hossain, A. I. Minett, S. X. Dou, V. G. Gomes, *J. Power Sources* **2016**, *328*, 472.
64. M. S. Islam, Y. Deng, L. Y. Tong, A. K. Roy, S. N. Faisal, M. Hassan, A. I. Minett, V. G. Gomes, *Mater. Today Commun.* **2016**, *10*, 112.
65. M. W. Haenel, *Fuel* **1992**, *71*, 1211.
66. R. Q. Ye, C. S. Xiang, J. Lin, Z. W. Peng, K. W. Huang, Z. Yan, N. P. Cook, E. L. G. Samuel, C. C. Hwang, G. D. Ruan, G. Ceriotti, A. R. O. Raji, A. A. Martí, J. M. Tour, *Nat. Commun.* **2013**, *4*, 2943.
67. Z. P. Zhang, J. Zhang, N. Chen, L. T. Qu, *Energy Environ. Sci.* **2012**, *5*, 8869.
68. S. R. Singamaneni, J. V. Tol, R. Q. Ye, J. M. Tour, *Appl. Phys. Lett.* **2015**, *107*, 212402.
69. Y. Q. Zhang, D. K. Ma, Y. Zhuang, X. Zhang, W. Chen, L. L. Hong, Q. X. Yan, K. Yu, S. M. Huang, *J. Mater. Chem.* **2012**, *22*, 16714.
70. Z. Z. Guo, L. G. Gai, J. H. Zhou, H. H. Jiang, Y. Tian, *Sens. Actuators B Chem.* **2016**, *232*, 722.
71. J. Zhou, X. Y. Shan, J. J. Ma, Y. M. Gu, Z. S. Qian, J. R. Chen, H. Feng, *RSC Adv.* **2014**, *45*, 5465.
72. Y. Z. Han, D. Tang, Y. M. Yang, C. X. Li, W. Q. Kong, H. Huang, Y. Liu, Z. H. Kang, *Nanoscale* **2015**, *7*, 5955.
73. S. Chandra, P. Patra, S. H. Pathan, S. Roy, A. Goswami, *J. Mater. Chem. B* **2013**, *1*, 2375.
74. Y. P. Hu, J. Yang, J. W. Tian, L. Jia, J. S. Yu, *Carbon* **2014**, *77*, 775.
75. S. G. Do, W. Kwon, Y. H. Kim, S. R. Kang, T. Lee, T. W. Lee, S. W. Rhee, *Adv. Opt. Mater.* **2016**, *4*, 276.
76. Y. Q. Dong, H. C. Pang, H. B. Yang, C. X. Guo, J. W. Shao, Y. W. Chi, C. M. Li, T. Yu, *Angew. Chem. Int. Ed.* **2013**, *125*, 7954.
77. X. J. Gong, W. J. Lu, Y. Liu, Z. B. Li, S. M. Shuang, C. Dong, M. M. F. Choi, *J. Mater. Chem. B* **2015**, *3*, 6813.
78. Y. Park, J. Yoo, B. Lim, W. Kwon, S. W. Rhee, *J. Mater. Chem. A* **2016**, *4*, 11582.
79. S. Ghorai, I. Roy, S. De, P. S. Dash, A. Basu, *New J. Chem.* **2020**, *44*, 5366.
80. Y. Q. Dong, J. P. Lin, Y. M. Chen, F. F. Fu, Y. W. Chi, G. N. Chen, *Nanoscale* **2014**, *6*, 7410.
81. S. Zhang, J. Y. Zhu, Y. Qing, C. W. Fan, L. X. Wang, Y. D. Huang, R. Sheng, Y. Guo, T. Wang, Y. L. Pan, Y. Lv, H. H. Song, D. Z. Jia, *Mater. Today Energy* **2017**, *6*, 36.
82. M. Saikia, J. C. Hower, T. Das, T. Dutta, B. K. Saikia, *Fuel* **2019**, *243*, 433.
83. R. Q. Ye, Z. W. Peng, A. Metzger, J. Lin, J. A. Mann, K. W. Huang, C. S. Xiang, X. J. Fan, E. L. G. Samuel, L. B. Alemany, A. A. Martí, J. M. Tour, *ACS Appl. Mater. Interfaces* **2015**, *7*, 7041.
84. C. Hu, C. Yu, M. Y. Li, X. N. Wang, J. Y. Yang, Z. B. Zhao, A. Eychmüller, Y.-P. Sun, J. S. Qiu, *Small* **2015**, *10*, 4926.
85. M. Y. Li, C. Yu, C. Hu, W. B. Yang, C. T. Zhao, S. Wang, M. D. Zhang, J. Z. Zhao, X. N. Wang, J. S. Qiu, *Chem. Eng. J.* **2017**, *320*, 570.
86. S. L. Hu, Z. J. Wei, Q. Chang, A. Trinchi, J. L. Yang, *Appl. Surf. Sci.* **2016**, *378*, 402.
87. S. K. Thiyagarajan, S. Ragupathy, D. Palanivel, K. Raji, P. Ramamurthy, *Phys. Chem. Chem. Phys.* **2016**, *18*, 12067.
88. B. Manoj, A. M. Raj, G. T. Chirayil, *Sci. Rep.* **2017**, *7*, 18012.
89. B. Manoj, A. M. Raj, G. C. Thomas, *Sci. Rep.* **2018**, *8*, 13891.
90. X. X. Liu, J. Y. Hao, J. H. Liu, H. C. Tao, *IOP Conf. Series* **2018**, *113*, 012063.
91. X. Meng, Q. Chang, C. R. Xue, J. L. Yang, S. L. Hu, *Chem. Comm.* **2017**, *53*, 3074.
92. Q. R. Liu, J. J. Zhang, H. He, G. X. Huang, B. L. Xing, J. B. Jia, C. X. Zhang, *Nanomaterials* **2018**, *8*, 844.
93. H. B. Wang, G. Q. Ning, X. He, X. L. Ma, F. Yang, Z. M. Xu, S. Q. Zhao, C. M. Xu, Y. F. Li, *Nanoscale* **2018**, *10*, 21492.
94. M. Q. He, X. R. Guo, J. Z. Huang, H. H. Shen, Q. Zeng, L. S. Wang, *Carbon* **2018**, *140*, 508.
95. X. T. Feng, Y. Zhang, *RSC Adv.* **2019**, *9*, 33789.
96. B. J. Geng, D. W. Yang, F. F. Zheng, C. Zhang, J. Zhan, Z. Li, D. Y. Pan, L. Wang, *New J. Chem.* **2017**, *41*, 14444.
97. N. Kundu, P. Bhunia, S. Sarkar, P. Biswas, *Opt. Mater.* **2020**, *100*, 109638.
98. H. L. Fei, R. Q. Ye, G. L. Ye, Y. J. Gong, Z. W. Peng, X. J. Fan, E. L. G. Samuel, P. M. Ajayan, J. M. Tour, *ACS Nano* **2014**, *8*, 10837.
99. L. Wang, H. Zhang, *J. Alloys Compd.* **2020**, *815*, 152502.
100. Y. T. Zhang, K. Zhang, K. Jia, G. Y. Liu, S. Z. Ren, K. K. Li, X. Y. Long, M. Li, J. S. Qiu, *Fuel* **2019**, *241*, 646.
101. B. Zhang, H. Maimaiti, D. D. Zhang, B. Xu, M. Wei, *J. Photoch. Photobio. A* **2017**, *345*, 54.
102. H. Maimaiti, A. Awati, D. D. Zhang, G. Yisilamu, B. Xu, *RSC Adv.* **2018**, *8*, 35989.
103. D. D. Zhang, H. Maimaiti, A. Awati, G. Yisilamu, F. C. Sun, *Chem. Phys. Lett.* **2018**, *700*, 27.
104. F. C. Sun, H. Maimaiti, Y. Liu, A. Awati, *Int. J. Energ. Res.* **2018**, *42*, 4458.
105. J. J. Zhang, Q. R. Liu, H. He, F. Shi, G. X. Huang, B. L. Xing, J. B. Jia, C. X. Zhang, *Carbon* **2019**, *152*, 284.
106. J. Yu, C. X. Zhang, Y. L. Yang, G. Y. Yi, R. Q. Fan, L. Li, B. L. Xing, Q. R. Liu, J. B. Jia, G. X. Huang, *New J. Chem.* **2019**, *43*, 18355.

107. Y. T. Zhang, K. K. Li, S. Z. Ren, Y. Q. Dang, G. Y. Liu, R. Z. Zhang, K. B. Zhang, X. Y. Long, K. L. Jia, *ACS Sustain. Chem. Eng.* **2019**, 9793.
108. Y. Xu, S. N. Wang, X. Y. Hou, Z. Sun, Y. Jiang, Z. B. Dong, Q. B. Tao, J. Man, Y. Cao, *Appl. Surf. Sci.* **2018**, *445*, 519.
109. S. L. Hu, X. Meng, F. Tian, W. L. Yang, N. Li, C. R. Xue, J. L. Yang, Q. Chang, *J. Mater. Chem. C* **2017**, *5*, 9849.
110. L. Wang, W. T. Li, M. Li, Q. Q. Su, Z. Li, D. Y. Pan, M. H. Wu, *ACS Sustain. Chem. Eng.* **2018**, *6*, 4711.
111. S. Kang, K. M. Kim, K. Jung, Y. Son, S. Mhin, J. H. Ryu, K. B. Shim, B. Lee, H. S. Han, *T. Song, Sci. Rep.* **2019**, *9*, 4101.
112. L. Nilewski, K. Mendoza, A. S. Jalilov, V. Berka, G. Wu, W. K. A. Sikkema, A. Metzger, R. Q. Ye, R. Zhang, D. X. Luong, T. Wang, E. McHugh, P. J. Derry, E. L. Samuel, T. A. Kent, A.-L. Tsai, J. M. Tour, *ACS Appl. Mater. Interfaces* **2019**, *11*, 16815.
113. A. Kovalchuk, K. Huang, C. S. Xiang, A. A. Marti, J. M. Tour, *ACS Appl. Mater. Interfaces* **2015**, *7*, 26063.
114. J. Y. Zhu, S. Zhang, L. X. Wang, D. Z. Jia, M. J. Xu, Z. B. Zhao, J. S. Qiu, L. X. Jia, *Carbon* **2018**, *129*, 54.

AUTHOR BIOGRAPHIES

Ziguo He is studying for a doctorate in Anhui University of Technology, and works in Tongling University. His research interests are focused on the design and preparation of novel coal-based nanomaterials, as well as their applications in sensing and bioimaging.

Cheng Zhang is assistant professor in Anhui University of Technology. He got a PhD from University of Science and Technology of China. His current research interests are focused on the design and synthesis of functional materials for environmental and enery application.

Zhicai Wang obtained his PhD degree from East China University of Science and Technology in 2007, and worked as professor at Anhui University of Technology in China from 2008. His research fields are coal chemistry and energy application.

Kui Zhang is professor at Anhui University of Technology in China. He got a PhD from University of Science and Technology of China in 2011 and worked as a research assistant at the Institute of Intelligent Machines, Chinese Academy of Sciences (2011-2015), and as a research fellow at the Center of Super-Diamond and Advanced Films (COSDAF) in the City University of Hong Kong (2015-2017). His research interests are in analytical chemistry, nanotechnology, and development of functional nanomaterials for chemo/bio sensing, environmental and energy application.

How to cite this article: He Z, Liu S, Zhang C, et al. Coal based carbon dots: Recent advances in synthesis, properties and applications. *Nano Select*. **2021**;*2*:1589–1604.
https://doi.org/10.1002/nano.202100019